PAPER

Bio-inspired robotic dog paddling: kinematic and hydro-dynamic analysis

Bioinspiration & Biomimetics

PAPER

Bio-inspired robotic dog paddling: kinematic and hydro-dynamic analysis

RECEIVED
10 March 2019

REVISED
16 August 2019

ACCEPTED FOR PUBLICATION
20 August 2019

PUBLISHED
13 September 2019

Yunquan Li[1], Frank Fish[2], Yonghua Chen[1,4], Tao Ren[3] and Jianshu Zhou[1]

[1] Department of Mechanical Engineering, The University of Hong Kong, Pokfulam Road, Hong Kong, People's Republic of China
[2] Department of Biology, 750 S. Church St., West Chester University, West Chester PA 19383, United States of America
[3] Robotics Research Center, Xihua University, Chengdu, Sichuan, People's Republic of China
[4] Author to whom any correspondence should be addressed.

E-mail: yhchen@hku.hk

Keywords: soft robotics, biomechanics, robotic dog, paddling gait, amphibous robotic dog

Supplementary material for this article is available online

Abstract

Research on quadrupedal robots inspired by canids or felids have been widely reported and demonstrated. However, none of these legged robots can deal with difficult environments that include water, such as small lakes, streams, rain, mud, flooded terrain, etc. In this paper, we present for the first time a kinematic analysis and a hydrodynamic model of dog paddling motion in a robotic system. The quadrupedal paddling gait of dogs was first analyzed based on underwater video recording. Hydrodynamic drag force analysis in a paddling gait cycle was conducted for a prototype robotic dog. The prototype robotic dog was developed using four pre-charged pneumatics soft actuators with consideration of relative positions of CG (center of gravity) and CB (center of buoyancy) and their dynamic variation in paddling. It was found that such soft actuators have great potential in developing amphibious legged robots, because they are inherently water-tight, anti-rusty, simple in structural design, and have large hydrodynamic advantage due to their mostly hemi-cylindrical shape design. Trotting and paddling of the prototype robotic dog was also demonstrated. It is believed that our findings reported in this research will provide useful guidance in future development of amphibious robotic dogs.

Introduction

Compared with wheeled robots, legged robots have better adaptability of different terrain [1]. Quadrupedal animals such as cats, dogs or cheetahs have inspired a lot legged robot developments [2–7]. Prime examples include Cheetah-Cub [2], BigDog [3], Spot Mini [4], MIT Cheetah [5], and StarlETH [6] etc. These robots can all maneuver in different gaits (walking, trotting and bounding) for various terrain conditions [7]. However, most existing quadrupedal robots were mainly developed for ground-based tasks. They lack waterproof bodies and are incapable of aquatic propulsion. When it comes to an unknown environment for tasks like resource exploration or disaster rescue [8], small lakes or streams may easily block their way. Amphibious robots are suitable for more diverse applications and can also deal with difficult environments [9], which include water in any form (for example rain, partially flooded terrains, and mud, etc) [10]. For most existing quadrupedal legged robots, amphibious design becomes a rather challenging topic: these robots usually require several motors or specific mechanisms (springs, linkage, etc) for actuation of each limb [11–13], therefore, the complete waterproofing requirements dramatically influence all aspects in the design process, rendering it more complex compared to dry-land robots [14]. What's more, operation in water environment can easily lead to rusting or corrosion of limbs with metal parts [15].

Researchers have reported many forms of amphibious robots [8, 14, 16–28]. Although these robots have favorable aquatic locomotion ability, their terrestrial movements are sacrificed and their dynamic locomotion ability can hardly coMPare with aforementioned quadrupedal robots. Some researchers employed two sets of propulsion mechanisms to achieve terrestrial and aquatic locomotion (i.e. AmphiRobot-I, AmphiRobot-II [14], and WhegsTM [17]). These

robots need extra propulsion mechanisms which lead to more complicated design and heavier weight. They apply wheels for on-land crawling and fin propeller mechanisms in water for fish-like swimming [8, 14, 17–20]. Snake-like robots were also developed for aquatic locomotion [21–23]. They possess undulating slender bodies and can propel themselves on land and underwater. However, their terrestrial movement flexibility and speed cannot match with the quadrupedal robots. Fish fin-based amphibious robots have a fin mechanism that can switch between fin and leg [8, 24]. The fins function as paddles during swimming and as legs while walking [25, 26]. Even though such robots are very efficient in swimming, their land mobility are also limited because the fin-leg design are too simple and not strong enough to generate effective terrestrial gaits. Another good example of an amphibious legged robot is the Salamander Robot [10]. It is a salamander-inspired amphibious robot that utilizes body undulation and leg walking to mimic the ability of salamanders to transit from terrestrial to aquatic locomotion [27, 28]. However, it is noted that only a crawling terrestrial gait is achievable in the salamander robot, which greatly limits its terrestrial mobility compared with other types of quadrupedal robots [2–6].

Seeking answers from nature, quadrupedal mammals frequently move across water and are thus able to swim [29]. For mammalian swimmers, their swimming modes were derived from terrestrial gaits [30]. The term 'dog paddle' representing the paddling gait, has been applied to the swimming motions of a number of both aquatic and terrestrial animal species such as water-rats, dogs, mink, etc. It is a modification of a terrestrial gait [31] as illustrated in figure 1(a). In a paddling gait cycle, the legs are accelerated posteriorly through an arc to generate an anteriorly-directed drag. The drag on the limb produces the thrust to translate the body forward.

In this research, we aim to develop a robotic dog that not only can trot on land, but also can paddle in water by only using its limbs, without any extra specific propeller mechanism. The trotting gait efficiency must not be influenced by the paddling gait just like a real dog. It is possible to generate a stable paddling gait if a quadrupedal robot design has considered the relative positions of CG (center of gravity) and CB (center of buoyancy) and their dynamic variation in a paddling gait cycle. Of course, construction of watertight body and limbs is a prerequisite for an amphibious robot. Because none of current robotic dogs have been developed with paddling capability, a self-contained, untethered and water-tight prototype robotic dog as shown in figures 1(b) and (c) was developed for the proposed analysis and demonstration. The prototype dog has one wireless camera mounted at the head, four legs based on soft pre-charged pneumatic (PCP) actuators [32]. In total, there are six servomotors: one for the mouth, one for the tail and four for the legs. All components including a battery, a control board and servomotors are mounted inside the body with consideration of the relative positions of CG and CB.

The proposed robotic dog uses novel PCP soft actuators [32] as legs for paddling and trotting gaits. The PCP actuator is a recently proposed soft actuator concept in our previous research [32, 33], it is light weight, with high degree of freedom movement, simple structure and easy to make just like making an ordinary pneumatic soft actuator. It is also proved to have several advantages over traditional PSA: high stiffness, better controllability, and not constrained by an air pump, etc. PCP soft actuators have great potential to amphibious robotic dog design because: firstly, PCP soft actuators are inherently waterproof, thus no cumbersome waterproof features need to be considered in the legs; secondly, PCP soft actuators are normally hemi-cylindrical, which can provide large hydrodynamic advantage; and thirdly, PCP soft actuators are buoyant themselves, eliminating the need for a large shell to enclose the robotic body; lastly, PCP soft actuators have high stiffness for fast on terrain gait such as trotting.

Major contributions of this paper are summarized as the following:

a. Hydrodynamic drag force analysis of robotic dog paddling;
b. Quantitative analysis of robotic dog paddling kinematics;
c. Novel design of an untethered amphibious robotic dog driven by soft PCP actuators.

Mechanical design of the robotic dog

Soft legs designed as PCP soft actuators

Figure 2(a) shows the working principles of the PCP soft actuator. The body design of the PCP soft actuator is similar with a traditional PSA (pneumatic soft actuator). The entire actuator body is made of silicone rubber, with an inextensible layer attached to the bottom of the actuator. The differences of the PCP soft actuator with PSA are: 1. tendon guides are molded on the upper side of the actuator, a tendon passes through the tendon guide and connects to a hard tip (3D printed foot). 2. The tube is connected with a check-valve to seal the pressured gas inside. When pressurized gas is injected and sealed inside the chamber, the actuator will bend downward (figure 2a(2)), we define it as pre-charged state. Then the actuator is pulled straight through the tendon by a pulling force F (figure 2a(3)). We can control the bending angle and bending speed of the PCP soft actuator by controlling the pulling/releasing tendon speed V and tendon length change x. The detailed 3D model and design parameters of the PCP soft leg are shown in figure 2(b). Length of bending part of the PCP soft leg is 110 mm. Radius of the air chamber cross-section is 12 mm, chamber thickness is 4 mm. Five tendon guides (thickness 8 mm, spacing

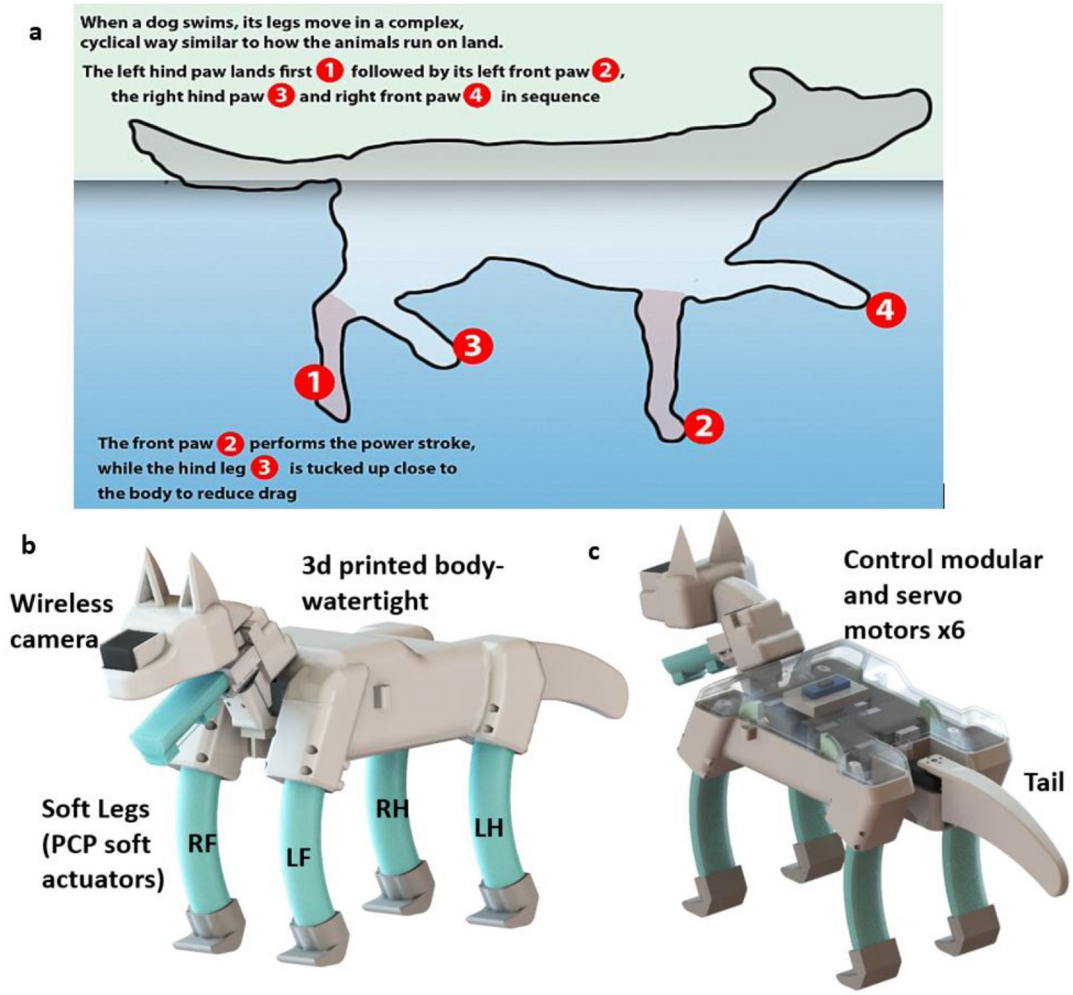

Figure 1. Dog paddling and prototype design illustration. (a) Illustration of dog paddling. (b) Exterior of the proposed robotic dog. The right fore leg, right hind leg, left fore leg, and left hind leg are indicated by RF, RH, LF, and LH, respectively. (c) Interior with a controller, six servomotors and a battery.

12 mm) are uniformly distributed on the back of the actuator. The tendons will pass through the tendon guides and be pulled together at one end to control the actuator. Distance between two tendon guide channels is 23 mm, and the distance of the tendon guide to the bottom layer is about 20 mm. We measure the pulling and releasing force using experiment setup as shown in figure 2c(1) with the soft leg prototype (force gauge installed on a linear guide, moving speed 10 mm s^{-1}). The leg will bend to 90° (at pre-charged air pressure 0.01 MPa). As shown in figure c(2), when pulling the leg straight from the 90° bending angle, the pulling distance D (equal to tendon length change x) is about 40 mm with the largest pulling force 25 N. The pulling force in the releasing process is smaller than the pulling process because of elastic hysteresis of the silicone rubber. The silicone rubber of the leg has a hardness SHORE A 20D. The hardness of the material decides the stiffness and bending angle of the PCP soft actuator under the same air pressure. A smaller hardness (e.g. SHORE A 10D) has larger bending angle, while the stiffness of the actuator is smaller. A larger hardness (e.g. SHORE A 30D) has a larger stiffness. However, it bends less under the same air pressure. The check-valve we use is AKH04-00. Nylon fishing line is used as tendons because of its high tensile strength (0.6 mm diameter, 22 kg pulling force). Manufacturing process of the PCP soft actuator is the same to that of a traditional PSA soft actuator.

In previous research [32], we have already analyzed and measured the relationship between the tendon's pulling distance/speed and the bending angle/speed based on a prototype design. The actuator design in this research has some difference from the previous version; specifically, unlike the previous version, the height and width of tendon guides are much smaller that it almost does not influence the expansion of the actuator. This makes the bending curve of the soft actuator smoother. Therefore, we simplify the geometrical bending model of the soft actuator as shown in figure 2(d). The actuator body is simplified as a whole body, where AB represents the tendon, CD represents the inextensible layer. In the pre-charged state, AB will elongate along with the upper layer of the soft actuator, the inextensible layer length CD remains unchanged. When the actuator is pulled straight, the length of CD is equal to AB ($l = 110$ mm). When releasing the tendon, the change of the tendon length is x, and the

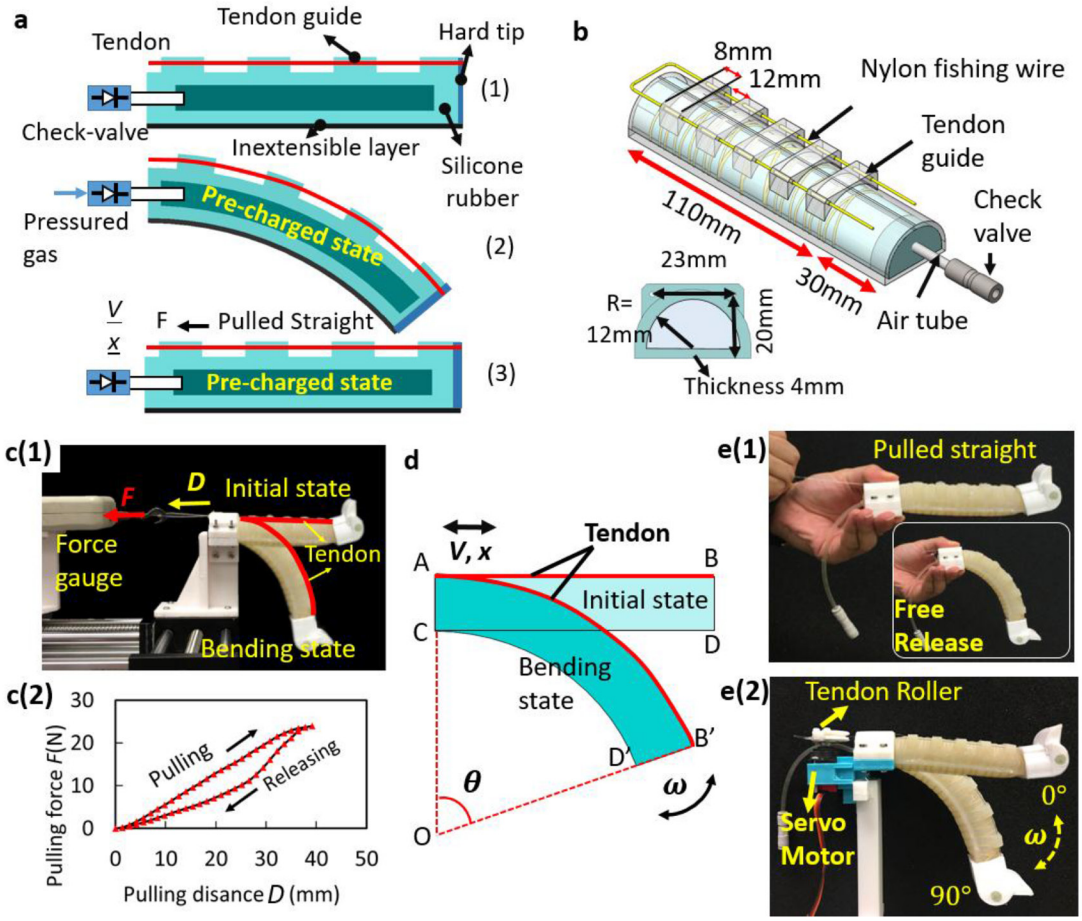

Figure 2. PCP soft leg. (a) Working principle of PCP soft actuator (b) 3D model and design parameters of the PCP soft leg. c(1) Pulling test of the leg prototype. c(2) Relationship of Pulling force F versus pulling distance D. (d) Kinematic model of the PCP soft leg. e(1) Free releasing test of PCP soft leg. e(2) Bending speed test with servomotor.

bending angle is θ. Other parameters can be seen in figure 2(b). At initial state, θ and x equal zero. During the bending process, x will increase with the increase of θ. Based on the assumptions, we can derive the relationship between the θ and tendon length change x.

$$\overset{\frown}{\mathrm{AB}}' = \mathrm{CD} + x = \theta \times (\mathrm{OC} + \mathrm{AC}). \quad (1)$$

Because the inextensible layer CD remains the same during bending, we have

$$\mathrm{CD} = \overset{\frown}{\mathrm{CD}}' = \theta \times \mathrm{OC}. \quad (2)$$

We can get the relationship of the bending angle and tendon length change x:

$$x = \mathrm{AC} \times \theta. \quad (3)$$

We define the bending speed as $\omega = \frac{d\theta}{dt}$, which is the changing rate of the bending angle. Thus, the bending speed ω can be calculated as:

$$\omega = \frac{dx}{dt} \times \frac{1}{\mathrm{AC}} = \frac{V}{\mathrm{AC}}. \quad (4)$$

Where AC equals to 20 mm in the prototype design. It can be seen from Equation (4) that bending speed ω is linearly proportion to the pulling tendon speed V. Therefore, it can be inferred that the tendon is pulled/released at a constant speed, the bending speed is constant.

The bending time of the PCP soft leg is necessary when analyzing the paddling gait and trotting gait. It depends on three factors: actuator design (dimensions, materials), pre-charged air pressure and servomotor rotation speed. We first measure the bending time that is decided by the soft leg intrinsic properties (material, air pressure) when the tendon is freely released (pre-charged pressure 0.01 MPa) as shown in figure 2e(1). The PCP soft leg is pre-charged 0.01 MPa pressure, and then pulled straight by hand. A high-speed camera (iPhone 6p, 240 Hps) is used to take video of the leg bending process. We measure the bending time it takes when bending angle reaches 90° for five times, and the average value is about 0.15 s. Then we use a servomotor (torque: 25 kg cm, rotation speed: 60°/0.1 s) to control the bending of the soft leg (figure 2e(2)). The servomotor needs to rotate 150° to completely release/pull the tendon so that the soft leg bends to 90° from straight state, and the shortest response time is about 0.4 s. We also measure the bending speed with two different servomotor rotation speed (2.08 rad s^{-1} and 0.75 rad s^{-1}) for 5 times using a high-speed camera. The video is analyzed with Kenova software. It is shown that the bending speed basically remains constant (1.22 rad s^{-1} and 0.44 rad s^{-1}) outside the very short acceleration/

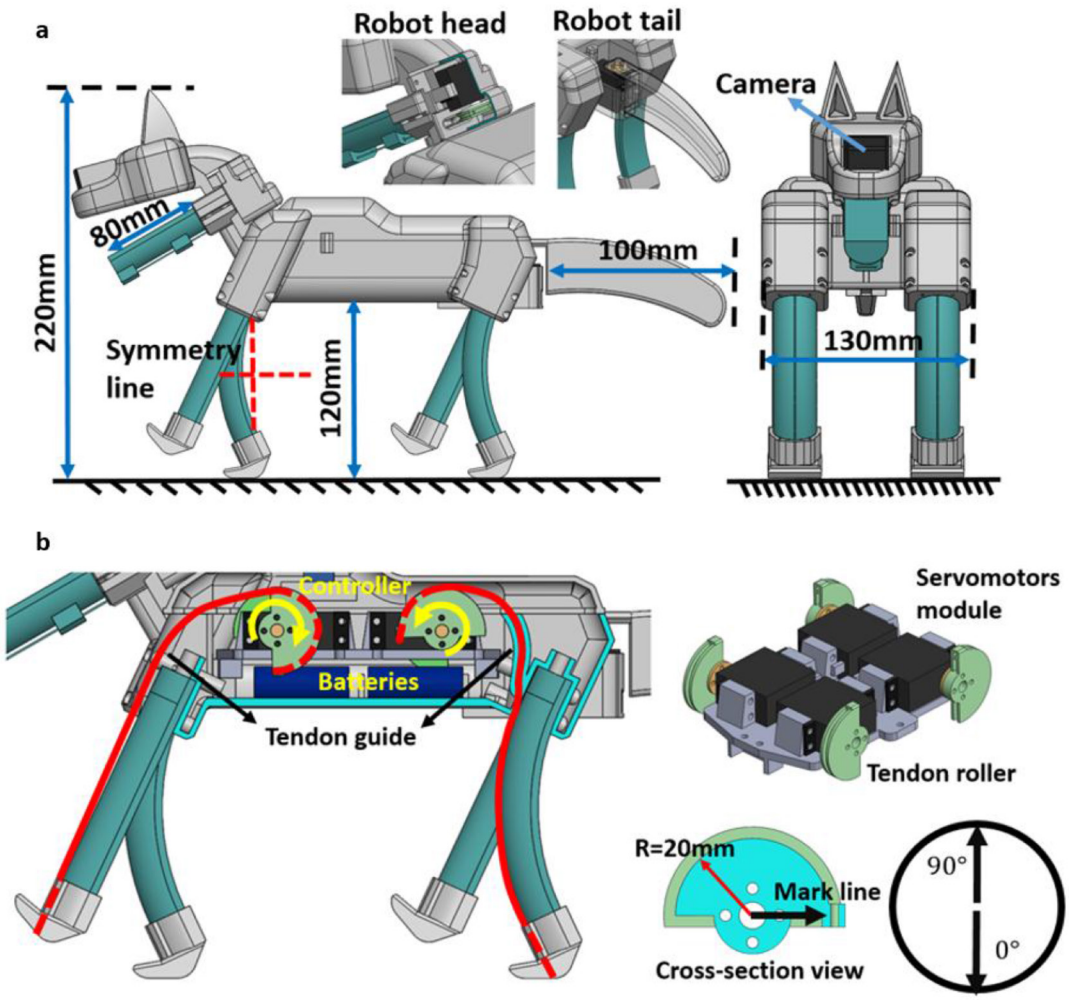

Figure 3. Mechanical design of the robotic dog. (a) Design parameters of the robotic dog. (b) Mechanical design of the power transmission system.

deceleration band when the servomotor is in control of the soft leg.

Overall design of the prototype amphibious robotic dog

Figure 3(a) shows the design parameters of the robotic dog. The torso, tail, and robotic head are 3D printed with PLA material. Body length of the robotic dog is about 53 cm, body width is about 16 cm. The limbs and the mouth are PCP soft actuator modules, each of them is controlled by a servomotor. Battery, controller, and four servomotors that control the limbs are all installed inside the torso, protecting them away from water. Servomotor for controlling the mouth is installed on the backside of the neck, inside a waterproof cover. When trotting on land, the bending angle of soft leg ranges in 0° to 90°, we set the installation angle of leg to be 25°. When the leg bends to half of the range (50°), the gravity line just passes through the foot point. This ensures that the gravity line lies in the range of bending leg. If the leg is installed vertical to the ground, trotting gait will be unstable because the gravity line lies in front of the leg. If the leg is installed with a larger angle, the trotting gait will also be unstable as the gravity line lies behind the foot points. Length of the tail is about 10 cm, which is one-fifth of the body length. The tail is designed to balance the head in water and to provide additional buoyancy, and the tail can be used as a rudder to steer the robot and control the swimming direction. The robot's tail is actuated by a waterproof servomotor with rotational range between 0° to 90°. A wireless camera is installed at the nose of the robotic dog for remote visual control.

Figure 3(b) shows the detail of the transmission mechanism of the limbs. From the cross-sectional view of the torso, the mechanical design of the inner structure is illustrated. One end of a robot limb is fixed inside the torso. Tendons passing through tendon guide (diameter 2 mm) are connected to the tendon roller, the tendon guide is filled with gear grease to prevent water coming inside the body. Four durable servomotors are installed on a servomotor support. The servomotor support is fixed with the torso to balance the tension force generated by the limb actuation. Tendon roller is a semicircle ($R = 2$ cm) wheel. We use 20 kg cm servomotors to control the soft limbs.

We take the tendon roller of LF (Left Fore) limb for example. The parameters of the tendon roller is

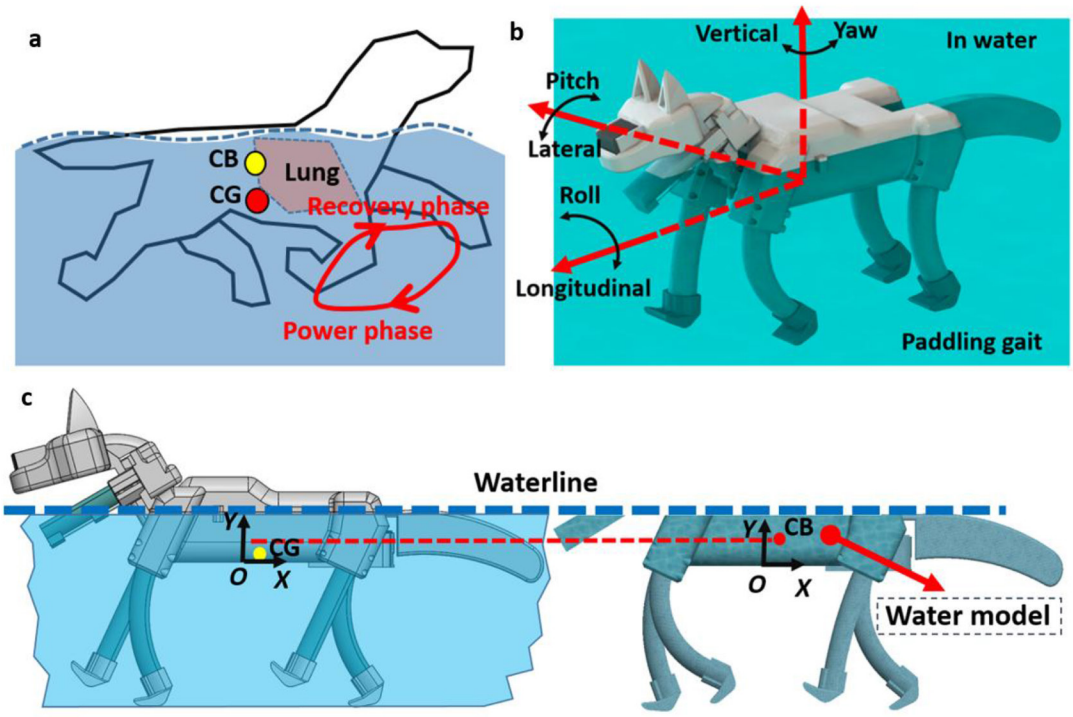

Figure 4. The amphibious robotic dog swimming analysis. (a) Outline of a dog swimming. (b) The six degree of freedom of the robotic dog in water. (c) Relative positions of CB and CG of the prototype robotic dog model.

designed to satisfy the condition: when the servomotor is at 0° position, the tendon is completely released and the soft leg is at fully bending state (current design has a maximum bending angle 90°); when the servomotor rotates to 150° position, the tendon is fully tensioned and the soft leg is held straight (bending angle 0°). Thus, the servomotor can control the bending speed, bending frequency and bending angle of the limb easily.

Figure 3(b) also shows that the battery and servomotor module are installed at the bottom part of the torso. An empty space is left in the upper torso, just as the dog's lung. This feature can bring down CG of the robotic dog, while raising CB at the same time.

Paddling gait analysis and implementation on robotic dog

Kinematic analysis of dog paddling

The biomechanics and energetics of the terrestrial and aquatic locomotion by mammals have been studied extensively [34–39]. It was found that a number of terrestrial and aquatic mammals apply the 'dog paddle' gait when swimming [29, 30, 38]. This paddling gait permits mammals to generate propulsive forces effectively while swimming at the water surface [34, 39]. In the present research effort, the paddling gait is inspired by dogs; in particular, we analyzed an underwater video [40] of a retriever swimming to model the kinematics of dog paddling.

Figure 4(a) shows an outline of a swimming dog indicating the positions of the body and legs and the locations of the CG and CB. Most of the body is submerged in the water, leaving only the head and dorsum of the body above surface of the water for observation and breathing. A dog's lungs are filled with air to provide positive buoyancy, and the legs are denser than the torso due to the high density from bones in the limbs. CG is located below CB as a lower CG can increase the stability of a floating body [41]. Based on the above observation, the amphibious robotic dog design should meet the following requirement: most of the robotic dog except the head should be submerged under the surface of the water to maintain dynamic stability in swimming with CG below CB.

Dynamic stability for robotic dog swimming is critical to maintain effective locomotor performance. Figure 4(b) shows the 3D model of the proposed robotic dog in water. It has six degrees of freedom (DOFs): three translational motions along longitudinal, lateral, and vertical direction, and three rotational motions in yaw, pitch and roll. For terrestrial locomotion, the solid ground can provide rigid support to the legs. Only translational movements in longitudinal and lateral directions, as well as the yaw rotation need to be considered. Other DOFs are constrained by the ground. Whereas for aquatic locomotion, pitch and roll are unconstrained, thus motion in these two directions must be considered. During the paddling gait, each leg will change its relative position to the robotic dog torso. This variation leads to variation of both the CG and the CB. The change of CG and CB will mainly lead to pitching of the robotic dog during swimming, inducing waves and turbulence which in turn affect dynamic stability in paddling.

Based on the 3D model of the robotic dog, its CG and CB can be easily found using a commercial software (SolidWorks2016). CG coordinate is calculated from the SolidWorks2016 by assigning material mass properties to the body parts (e.g. body shell, the soft legs, battery, controller, servomotors, etc). For a floating body, CB is defined as the CG of the displaced water. Therefore, for CB calculation, the submerged part of the dog is assigned as 'water model' (as shown in figure 4(c)), and then the CG of the 'water model' can be calculated by SolidWorks2016. Figure 4(c) shows the relative CG and CB positions of the 3D robotic dog model for a given posture projected on the sagittal plane. The robotic dog is designed to make the CG slightly below CB to increase the stability of the floating robotic dog.

Figure 4(a) illustrates the motion of the right fore limb of the dog model during a paddling cycle. All limbs are oriented underneath the body and moved through an arc. The trajectory has two phases: the power phase and the recovery phase. In the power phase, the limb extends and strokes rearward through and arc to its extreme position. In the recovery phase, the limb will retract to the torso and then extend forward to the initial position of power phase. It is known that the power phase of a paddling gait cycle was shorter than the recovery phase for both fore and hind limbs. According to the paddle footfall data from the online published document 'Dog Paddle Footfall Data' by Fish [42], for each limb, the power phase takes approximately 0.25 cycle time, and the recovery phase takes approximately 0.75 cycle time. This results in a greater velocity during power phase than that of the recovery phase. This difference in velocity between stroke cycle phases generates the drag-derived thrust and decreases the resistive drag during the recovery phase [34].

The gait cycle is constructed by analyzing the real mammals' paddling gait sequence (the order of leg movement). Most mammals use trotting gait sequence (diagonal limbs have same movement, limbs on same side have opposite movement, LF(RH)—RF(LH)) when paddling. However dogs use a different sequence (run sequence, LF—RH—RF—LH) in water because they try to avoid foot on the same side interact with each other. In a trotting sequence, when the diagonal limbs bend backward to push water, the other two limbs bend forward. For our robotic dog, because the limbs cannot tackle to the torso, the drag force will be almost the same as the thrust force because limbs bends/unbends at the same speed. As a result, the robotic dog just moves slightly forward and backward repeatedly and stay almost at the same place in a trotting cycle. If we slow down the unbending speed to 1/3 of the bending speed, pitching will be observed during paddling because of two reasons: 1. the position of limbs cannot keep the body in balance during paddling because two limbs have already bent back ward while the other two limbs are still unbending. 2. the lift forces are not eliminated. What's more, trotting sequence will cause a stop-go swimming because the stroke limbs need to wait the recovery limbs for some time. After several trail, for our robotic dog paddling, we let one limb thrust the water at one time while the other three limbs are in different state of recovery phase. Such a gait sequence can avoid pitching in paddling, and at the same time, provide a continuous forward motion.

Figure 5(a) shows a paddling gait cycle we designed and it is divided into four equal intervals. The relative bending angle of each limb (left fore leg (LF), right fore leg (RF), left hind leg (LH), and right hind leg (RH)) is shown in the figure. Take limb LH for example, during the power phase (0–1), the limb bends from 0° to 90°; during the recovery phase (1–4), the limb retracts from 90° to 0°.

We define the mid-point of the connection line between the fore and hind leg bases as the origin of the coordinate XOY as shown in figure 4(c). During a paddling gait cycle as in figure 5(a), the CG and CB of the robotic dog will change as the change of limb positions. Applying the previous discussed CG and CB measuring method, we measure the CG and CB variation by changing the four limbs' bending angles of the robotic dog model and the related 'water model' in SolidWorks2016. We analyze the stability of a floating body inside water first (figure 5(b)). It is known that the CG should be under CB a distance d for stable floating. When there is disturbance, the floating body will return to its balance position under combined torque of buoyancy force and gravity force. It can be seen that a larger d can provide better stability because the deviation angle is smaller under the same deviation displacement. For our robotic dog design, the distance d is designed to be 5 mm, as if the CG is too low, the legs will too heavy for trotting gait. During a paddling gait, four limbs are changing their bending angles at the same time. Therefore, the CG and CB will change their relative positions on the robotic dog body. We define x and y as the relative displacement of CB to CG, we can calculate the moment of CG to CB during paddling, based on calculation we can estimate the stability of robotic dog during paddling. Figures 5(c) and (d) shows the variation of the CG and CB in a paddling gait cycle (from interval 1 to 4). It can be seen that the variations for both CG and CB are relatively small (smaller than 2 mm) in a gait cycle. For variation in the Y direction, it does not cause any rotational effect. For variation in X direction, pitching may occur due to the shift in CG and CB. Take the first quarter of the gait cycle as an example, the difference between the CG and CB in X direction results in a moment, causing the robotic dog to pitch. The moment can be approximately represented as $|X_{CB1} - X_{CG1}| \times (F_b)$. From figures 5(c) and (d), X_{CG1} and X_{CB1} are 20.8 mm and 18.0 mm, respectively. F_b is the buoyancy of the dog. For the prototype dog, F_b is 23 N from SOLIDWORKS modelling. As a result, the pitching moment is $|18.0 - 20.8| \times 23 \times 1010^{-3}$ Nm, or 0.06 Nm. For the other three intervals, the pitching moments

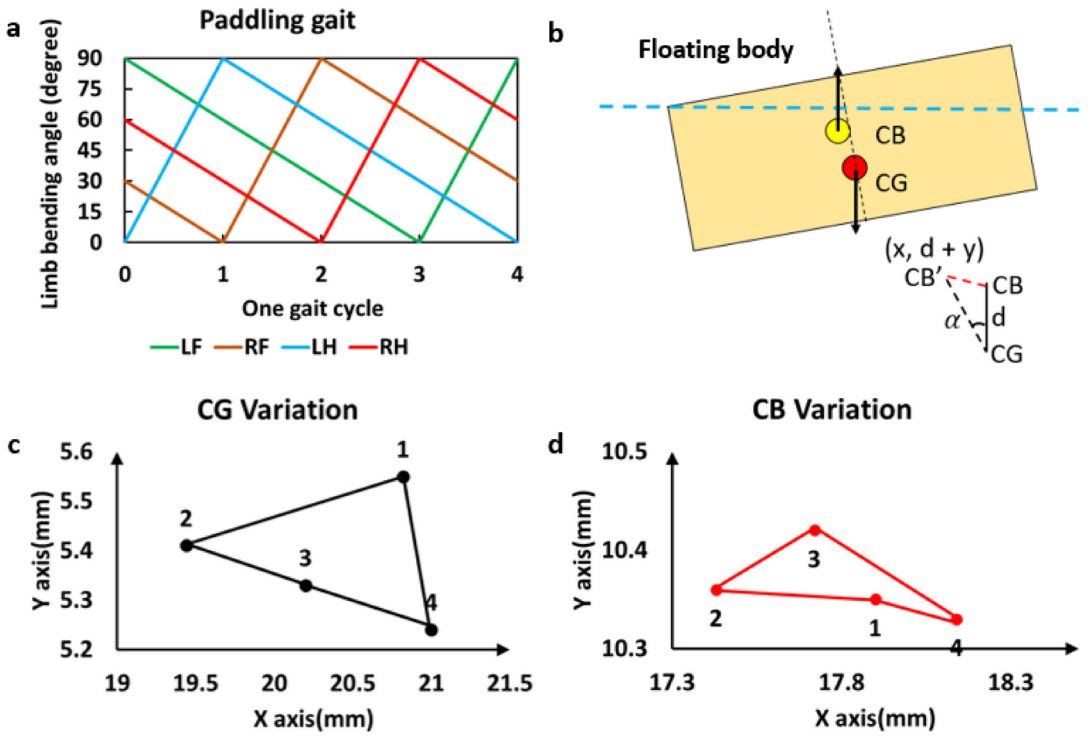

Figure 5. Analysis of a paddling gait cycle. (a) Limb motion in a paddling gait cycle. (b) Floating body stability (c) CG variation pattern. (d) CB variation pattern.

are, respectively, 0.051 Nm, 0.057 Nm and 0.067 Nm. Because the prototype dog has a large length, approximately 0.7 m, the influence of the pitching moment is not obvious in paddling.

Hydrodynamic drag force analysis of robotic dog paddling

'Dog paddling' is a drag-based swimming gait. To illustrate the paddling gait of a robotic dog, we first analyze the force condition of one limb in a paddling gait cycle. Each limb moves back and forth during paddling, corresponding to the power phase and recovery phase, respectively. Figures 6(a) and (b) shows the thrust force and drag force analysis of a limb during one paddling cycle. The range of movement in the vertical plane for the robotic limb is designed in range from 0° to 90°. Based on the paddling gait in figure 5(a), the power phase (limb moves from 0° to 90°) is 0.25 of the paddling cycle, and the recovery phase is 0.75 of the paddling cycle (limb returns to 0° position). We assume that the bending speed (angular velocity) of a limb is constant in the power phase (ω_1) and in the recovery process (ω_2).

In the power phase, the limb swings rearward to push the robotic dog forward. Reaction force (shown as red arrows) from the water is distributed along the limb, as shown in figure 6(a). Taking a force element near the foot as an example, it can be decomposed into the horizontal thrust force and vertical lift force. In the recovery phase, the limb swings forward, generating a resistance to the dog's forward motion. The resistance force is also distributed along the limb as shown in figure 6(b). A resistance force element near the foot is decomposed into the horizontal drag force and vertical lift force. In order to move forward, the thrust force from the power phase should be much larger than the drag force from the recovery phase. We analyze these two forces based on the drag force equation equation (1) from [43].

$$F = \frac{1}{2}\rho u^2 C_d A. \tag{5}$$

Where F is the drag force or thrust force from fluid, ρ is the density of the fluid (water is assumed), u is the relative speed of the liquid flow to the object, C_d is the drag coefficient (a dimensionless coefficient related to the object's geometry), and A is the reference area (orthographic projection of the object to the direction of motion). In this case, the projection plane is perpendicular to dog moving direction: the limb projection area for the power phase is $A_1 = W \times L_1$ (figure 6(a)); and projection area for recovery phase is $A_2 = W \times L_2$ (figure 6(b)), where L_1 and L_2 represent the length of the robot limb projection on the projection plane. For the above parameters, the density of the liquid ρ is a constant 1000.0 kg m^{-3} (water is assumed). Because the limb bends around the limb base point O, the flow speed u at each part of the limb is different. For a given position on the limb, the flow speed can be approximately calculated from $u = R\omega$, where R is the distance to the point O, ω is the angular bending velocity of the limb (where $\omega_1 = 1.22$ rad s^{-1}, $\omega_1 = 0.44$ rad s^{-1}).

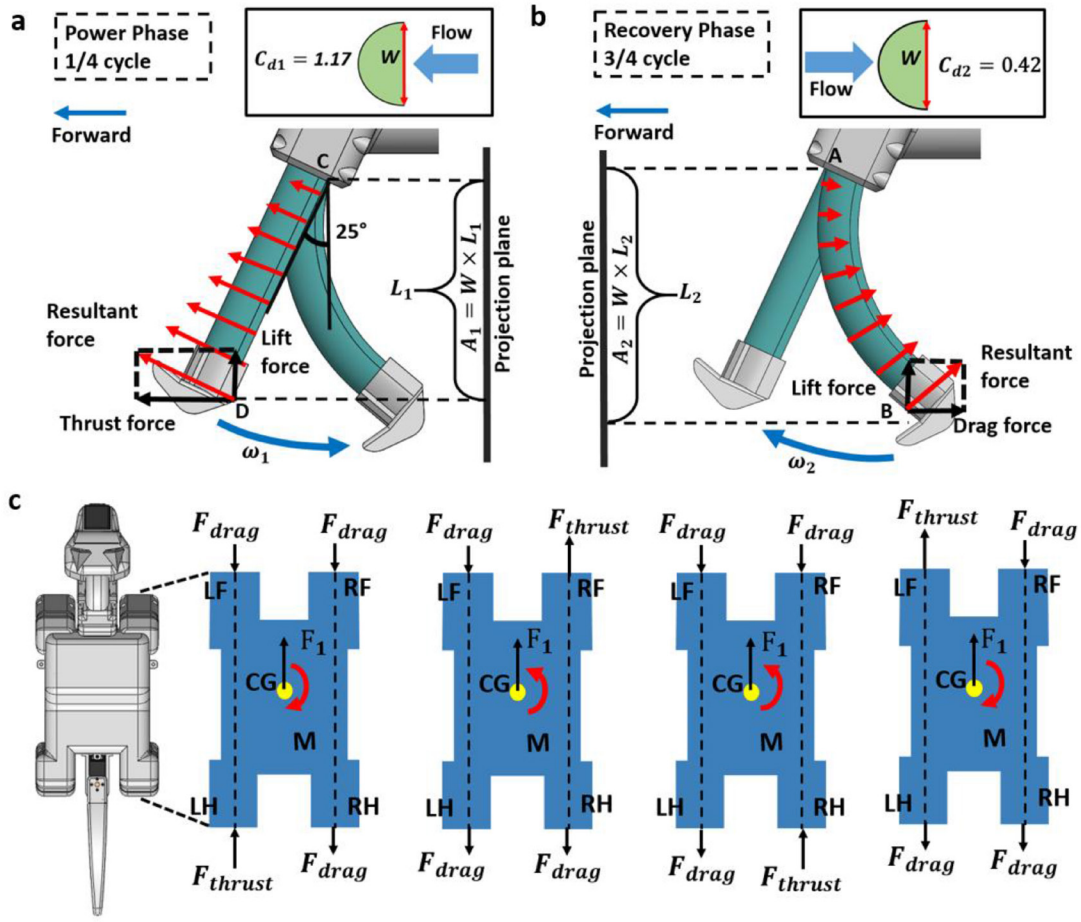

Figure 6. Force analysis in a paddling gait cycle: (a) force analysis during power phase. (b) Force analysis during recovery phase. (c) Limb forces in a paddling gait cycle.

Lift forces during power and recovery phases does not contribute to the forward motion, instead they cause pitching of robotic dog along the lateral axis, which is not good for stable paddling movement. Unlike the thrust/drag force, it should be noted that lift force changes its direction in both the power and the recovery phase when the leg bends from $0° - 90°$ (or $90° - 0°$). More specifically, in a power phase, when bending from $0° \sim 25°$, the lift force points downward, when bending from 25° to 90°, the lift force points upward and become resistance force. In the recovery phase, lift force points downward from 90° to 25°, and points upward from 25° to 0°. The vertical lift force is similar with the thrust force and drag force during paddling (smaller than 0.1 N). However, they are much smaller compared with the weight (2.3 kg, about 23 N) of the robotic dog. What's more, the robotic dog has a body length of 700 mm. The buoyancy force, almost uniformly distributed along the body, increase its stability when there is disturbance. Therefore, in our analysis, the lift forces are neglected.

A special feature of the limb deserving more discussion here is the hydrodynamic advantage. For soft actuators (the limbs in this study), the cross section is normally designed as a semi-circle as shown in the right corner of figure 6(a). In the power phase, the flat surface on the limb is subject to reaction force from the water. According to [44], the drag coefficient C_d for a flat surface is 1.17 (figure 6(a)). In the recovery phase, the hemi-cylindrical surface of the limb is subject to a reaction force from the water. The drag coefficient C_d for the hemi-cylindrical surface is 0.42 (figure 6(b)) based on [44]. According to equation (1), the hydrodynamic advantage of the limb design is 1.17/0.42, or 2.79. That is, when all conditions are the same, the thrust force of the limb is 2.79 times as much as the drag force. The large hydrodynamic advantage is necessary to increase propulsive efficiency and to generate enough thrust to overcome the drag on the torso. The drag on the torso is due to frictional, pressure and wave drag components [30, 31]. This finding is important for future design of robotic dog limbs if the robotic dog is also intended for paddling apart from land motion.

Figure 6(c) analyzes the limb force conditions of the robotic dog during a paddling gait cycle (divided into four equal intervals). The forces are shown on a horizontal plane. Based on the analysis in figures 6(a) and (b), in each quarter of the gait cycle, one limb generates thrust force, and the other three limbs generate drag forces. The approximate resultant force F_1 on the horizontal plane can be represented as $F_1 = F_{\text{thurst}} - 3F_{\text{drag}}$. These forces also generate a moment M along the CG as shown in figure 6(c). To propel the robotic dog forward, the resultant forces

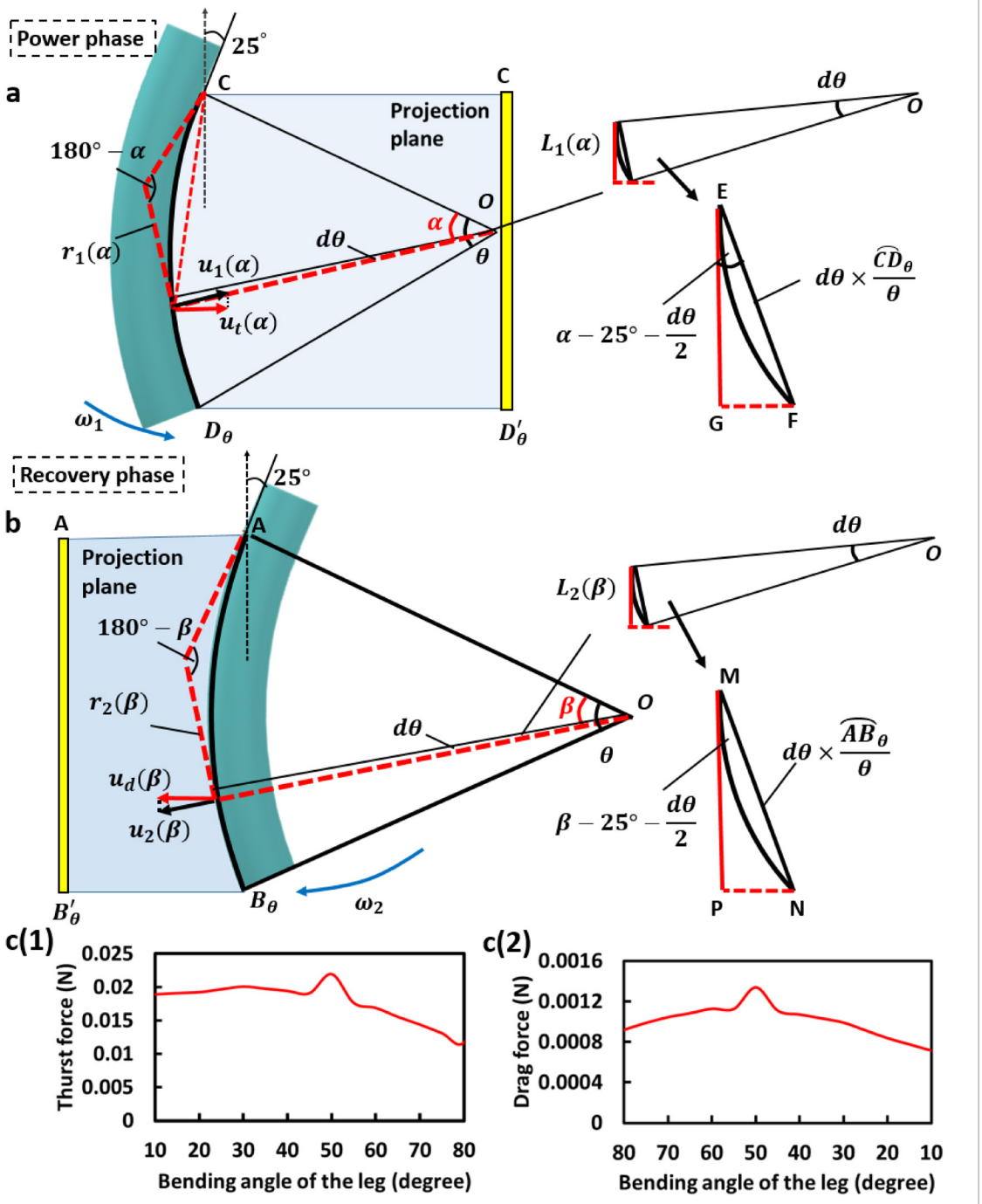

Figure 7. Thrust and drag force calculation: (a) analysis of the thrust force during power phase. (b) Analysis of the drag force during recovery phase. c(1) Thrust force curve versus limb bending angle. c(2) Drag force curve versus limb bending angle.

F_1 should always point forward. Directions of the moment M varies within a gait cycle (twice clockwise and twice counterclockwise), thus the rotational effect are canceled out in a paddling gait cycle.

During power/recovery phase, the bending angle of the soft leg changes, therefore, paddling projection area length are changing along with the bending angle. The thrust and drag force also change along with the bending angles. Which means the thrust/drag forces are function of the bending angle θ. Figures 7(a) and (b) shows the power phase and recovery phase of limb when bending angle equals to a random value θ, where $\theta \in (0°,\ 90°)$. It should be noted that the soft limb has a continuous bending curve, although the bending angular speed $\omega_1(\omega_2)$ is same for the entire soft leg, the bending linear speed is different at different positions on the limbs. As a result, equation (5) cannot be used directly for calculating the thrust and drag forces.

We use integral method to calculate the thrust/drag force when bending angle reaches θ by using the following functions:

$$F_{\text{thrust}}(\theta) = \int_0^{\theta} \frac{1}{2}\rho C_{\text{d1}} W L_1(\alpha)\left(u_t(\alpha) - v_{\text{dog}}\right)^2, \quad \text{where } \alpha \in (0°,\ \theta],\ \theta \in (0°,\ 90°) \tag{6}$$

$$F_{\text{drag}}(\theta) = \int_0^{\theta} \frac{1}{2}\rho C_{d2} W L_2(\beta)\left(u_d(\beta) + v_{\text{dog}}\right)^2, \quad \text{where } \beta \in (0^\circ,\ \theta],\ \theta \in (0^\circ,\ 90^\circ), \tag{7}$$

where $L_1(\alpha)$ is the vertical projection length of the unit limb curve at position α, $u_t(\alpha)$ is the relative horizontal thrust speed of the unit length limb at position α, and $L_2(\beta)$ is the vertical projection length of the unit limb curve at position β, $u_d(\beta)$ is the relative horizontal drag speed of the unit length limb at position β; v_{dog} is the speed of robotic dog during paddling.

Based on geometrical relationships, we have

$$L_1(\alpha) = \text{EF}\cos\left(\alpha - 25^\circ - \frac{d\theta}{2}\right) = \frac{d\theta}{\theta}\overset{\frown}{\text{CD}}_\theta \cos\left(\alpha - 25^\circ - \frac{d\theta}{2}\right) \tag{8}$$

$$L_2(\beta) = \text{MN}\cos\left(\beta - 25^\circ - \frac{d\theta}{2}\right) = \frac{d\theta}{\theta}\overset{\frown}{\text{AB}}_\theta \cos\left(\beta - 25^\circ - \frac{d\theta}{2}\right) \tag{9}$$

$$u_t(\alpha) = 2\omega_1 r_1(\alpha)\cos(|\alpha - 25^\circ|) \tag{10}$$

$$u_d(\beta) = 2\omega_2 r_2(\beta)\cos(|\beta - 25^\circ|), \tag{11}$$

where $d\theta$ is the unit angle and it is extremely small, therefore we have $\text{EF} \approx \overset{\frown}{\text{EF}} = \frac{d\theta}{\theta}\overset{\frown}{\text{CD}}_\theta$, $\text{MN} \approx \overset{\frown}{\text{MN}} = \frac{d\theta}{\theta}\overset{\frown}{\text{CD}}_\theta$ and $\frac{d\theta}{2} \to 0$; $\overset{\frown}{\text{AB}}_\theta = \overset{\frown}{\text{CD}}_\theta + 20\,\text{mm} \times \theta$, $r_1(\alpha)$ and $r_2(\beta)$ are the radius of bending speed, and based on geometry relationship, we have

$$r_1(\alpha) = \frac{\overset{\frown}{\text{CD}}_\theta}{\theta}\tan\frac{\alpha}{2},\ \alpha \in (0,\ \theta] \tag{12}$$

$$r_2(\beta) = \frac{\overset{\frown}{\text{AB}}_\theta}{\theta}\tan\frac{\beta}{2}, \beta \in (0,\ \theta]. \tag{13}$$

Based on the above equations, substitute (12) and (13) into equations (10) and (11), and then substitute (9)–(12) into (6) and (7). We can derive the expression of the thrust force F_{thrust} and drag force F_{drag} at bending angle θ.

$$F_{\text{thrust}}(\theta) \approx \int_0^{\theta} \frac{1}{2}\rho C_{d1} W \frac{d\theta}{\theta}\overset{\frown}{\text{CD}}_\theta \cos(\alpha - 25^\circ)\left(2\omega_1 \frac{\overset{\frown}{\text{CD}}_\theta}{\theta}\tan\frac{\alpha}{2}\cos(|\alpha - 25^\circ|) - v_{\text{dog}}\right)^2, \quad \text{where } \alpha \in (0^\circ,\ \theta],\ \theta \in (0^\circ,\ 90^\circ) \tag{14}$$

$$F_{\text{drag}}(\theta) \approx \int_0^{\theta} \frac{1}{2}\rho C_{d1} W \frac{d\theta}{\theta}\overset{\frown}{\text{AB}}_\theta \cos(\beta - 25^\circ)\left(2\omega_1 \frac{\overset{\frown}{\text{AB}}_\theta}{\theta}\tan\frac{\beta}{2}\cos(|\beta - 25^\circ|) + v_{dog}\right)^2, \quad \text{where } \beta \in (0^\circ,\ \theta],\ \theta \in (0^\circ,\ 90^\circ)\ . \tag{15}$$

In equations (14) and (15), ρ equals to $1000\,\text{kg m}^{-3}$, $C_{d1} \approx 1.17$, $C_{d2} \approx 0.42$, $W = 33\,\text{mm}$, $\overset{\frown}{\text{CD}}_\theta$ equals to 110 mm, $\overset{\frown}{\text{AB}}_\theta$ equals to 100 mm + 20 mm × θ. At the beginning of dog paddling, the speed of dog v_{dog} is very small, therefore we take the v_{dog} as zero. We can get the relationship curve between F_{thrust} and F_{drag} and the limb bending angle θ during the power phase and the recovery phase, respectively, as shown in figures 7c(1) and c(2). The thrust force during power phase varies in an interval 0.01 N–0.023 N, with the largest thrust force 0.023 N occurs at bending angle around 50°. The average value of the thrust force is 0.018 N. The drag force during the recovery phase varies in the interval 0.0008 N–0.0013 N, with the largest drag force 0.0013 N located at a bending angle around 50°. The average value of the drag force is 0.0009 N. In figure 6(c), for every quarter gait cycle, only one limb is in power phase, the other three limbs are all in recovery phase. We can calculate the average resultant force F_1 during one gait cycle, that is $F_1 = F_{\text{thurst}} - 3F_{\text{drag}} \approx 0.0153$ N. Based on this analysis, during the paddling gait cycle, the limbs can always generate a forward propulsion to the robotic dog.

When paddling forward, the water flow will generate a drag force to the robotic torso. The projection area of the submerged torso is shown in figure 8(a). For the purpose of drag force calculation, the shape of the torso is simplified to a cuboid (figure 8(b)). Therefore, the drag coefficient for the torso is $C_{d3} \approx 1.05$. At equilibrium state of constant swimming velocity, the thrust force will be equal to the drag forces generated by both the limbs and the torso.

That is,

$$F_{\text{drag\_torso}} + 3F_{\text{drag\_legs}} = F_{\text{thurst\_leg}}. \tag{16}$$

Based on equation (16), we can find the largest velocity that the robotic dog can finally reach.

We have the following equation:

$$\frac{1}{2}\rho C_{d3} A_{\text{torso}}\left(v_{\text{dog}}\right)^2 + \frac{3}{2}\rho C_{d2} A_2\left(u_d + v_{\text{dog}}\right)^2 = \frac{1}{2}\rho C_{d1} A_1\left(u_t - v_{\text{dog}}\right)^2. \tag{17}$$

From equation (17), when $v_{\text{dog}} > 2.5\,\text{cm s}^{-1}$, the overall drag forces will be larger than the thrust force. Therefore, the theoretical largest swimming velocity is about $2.5\,\text{cm s}^{-1}$.

The paddling gait is implemented on a prototype robotic dog as shown in figure 8(c). The test is conducted in an inflatable pool (1.25 m × 0.8 m). The robotic dog can swim forward without obvious pitching. The swimming speed is about $2.1\,\text{cm s}^{-1}$, or $75.6\,\text{m h}^{-1}$. The forces encountered at the air–water interface for non-piscine vertebrates are more complex and larger than those of submerged swimmers [30, 31].

Trotting gait planning

The rhythmic locomotor gaits of animals present high stability and adaptability. Rhythmic terrestrial gaits include trotting, walking, pacing and bounding, etc

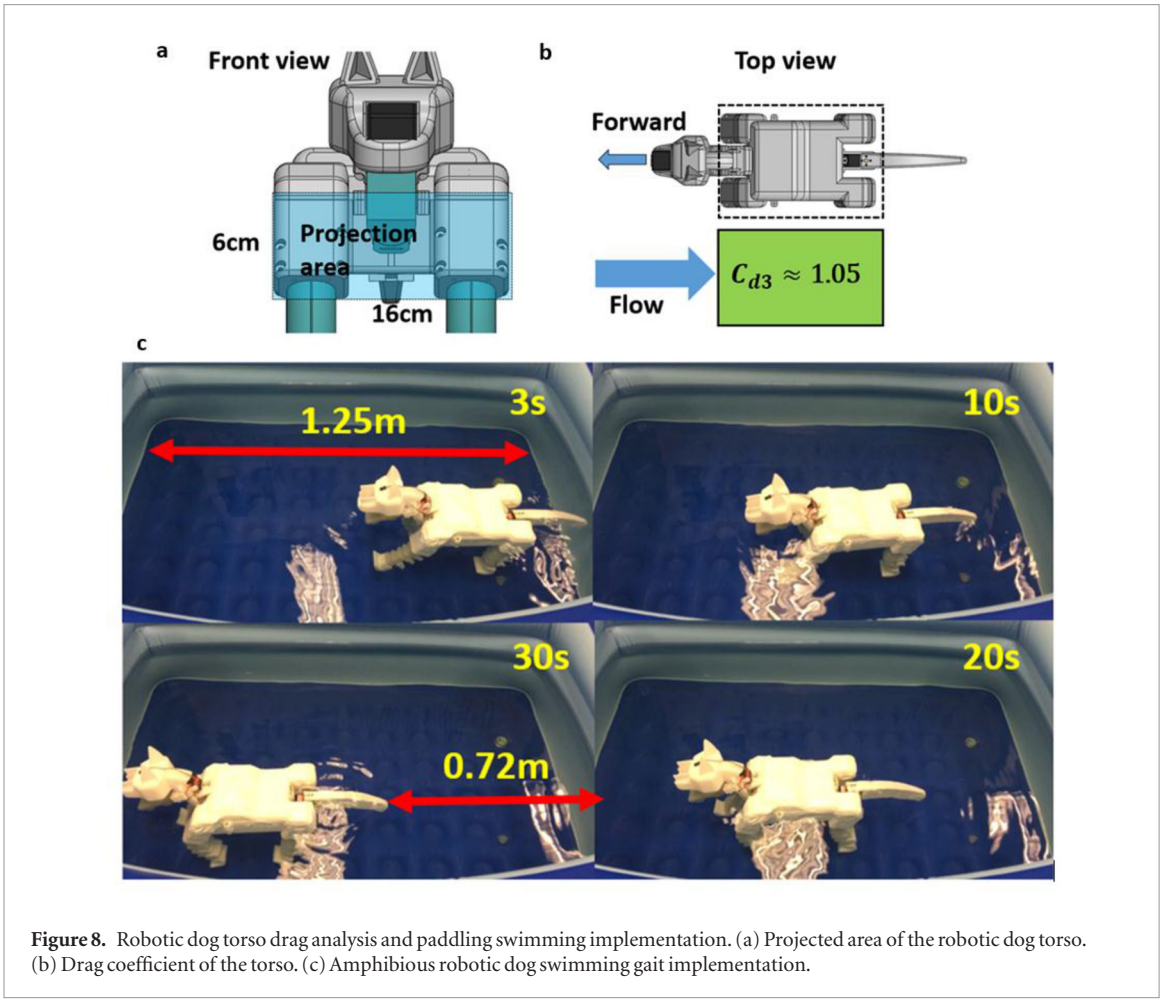

Figure 8. Robotic dog torso drag analysis and paddling swimming implementation. (a) Projected area of the robotic dog torso. (b) Drag coefficient of the torso. (c) Amphibious robotic dog swimming gait implementation.

[24]. As a moderate speed gait, trotting gait is the most efficient gait of the terrestrial gaits compared with other terrestrial gaits for quadrupedal animals [45, 46]. In a typical trotting gait cycle, diagonal pairs of feet are put down or pushed off the ground simultaneously. The diagonal motion pattern is considered to provide mechanical stability for the robot [47]. Figure 9(a) shows a possible way to generate a trotting gait for the prototype robotic dog. The trotting gait is planned with four steps. In step (1) and step (3), four legs are all in the neutral state. Two pairs of diagonal legs LF and RH in step (1), RF and LH in step (3) are contracting to compress pneumatic energy, lifting the corresponding feet up to reduce the friction force with the ground. The other two pairs of diagonal legs RF and LH in step (1), LF and RH in step (3) are extending to release pneumatic energy, pushing the body upward and forward. In step (2) and step (4), LF and RH in step (2), RF and LH in step (4) are in an 'energy stored' state, they are also away from contact with the ground by a distance ΔH. RF and LH in step (2), LF and RH in step (4) are fully extended and all of the pneumatic energy is released. In step (1) and step (3), the legs LF and RH in step (1), RF and LH in step (3) start to transit from 'energy stored' state to 'energy released' state simultaneously. The locomotion is powered by alternation pneumatic energy transition. As shown in figure 9(a), forward motion occurs between step (1) and step (2), step (3) and step (4), where pneumatic energy drives the locomotion.

Figure 9(b) shows the trotting state of the robotic dog 3D model, corresponding to the step (4) in figure 9(a). It can be seen that only two diagonal legs support the body. Figure 9(c) shows the leg design to parameters to meet the trotting gait requirement. When lift the feet up, the friction force should be small, and when the leg extend and push the ground, the feet should be able to provide support. The leg is installed 25° to vertical line, and the robotic dog stand at leg bending of 50°. During the trotting gait, the leg will bend to 60°–70° to provide some forward motion. When the leg is straight, it is lifted up from the ground for about 15 mm to ensure there is no contact between the feet and ground. Foot design is shown on the right corner of figure 9(c), where the toe of the leg is tilted up slightly, and the bottom of the foot is a small flat and smooth surface. The design of the foot is to reduce the friction force of the toe. A piece of rubber is attached to the heel of the foot to increase the friction when the leg bends and pushes rearwards.

The trotting speed is controlled by changing the rotation speed of the servomotors. According to the trotting gait planning, a control program has been implemented for the prototype based on the signal shown in figure 9(d), where signal pattern of one gait cycle is illustrated. In a cycle of the trotting gait,

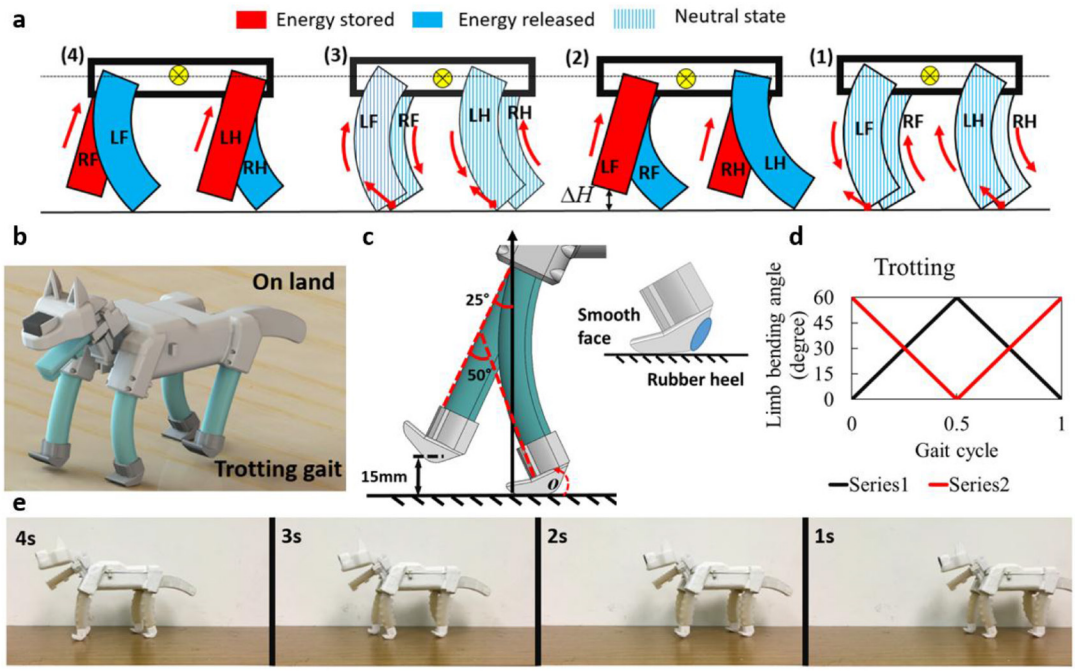

Figure 9. Trotting gait analysis and implementation. (a) Trotting gait analysis. (b) Robotic dog model trotting state. (c) Leg design parameters for trotting. (d) Trotting gait control signal. (e) Trotting gait implementation on robotic dog prototype.

the LF and RH bend in the same way, from 0° to 60° during the first half cycle, and 60° to 0° during the second half cycle. In the same cycle, servos for RF and LH rotate in a way that is exactly opposite to LF and RH. Figures 9e(1s) to e(4s) show the actual trotting gait of the prototype. The current prototype has the fastest trotting speed of 18 cm s^{-1}. This is sufficient to demonstrate the trotting capability of the proposed robotic dog.

Discussion

In this paper, we analyze the paddling kinematics and dynamics of dogs. For better illustration, a prototype robotic dog has been developed. The prototype robotic dog is capable of two typical gaits: trotting gait for terrestrial locomotion and paddling gait for aquatic locomotion. The robotic dog has four soft limbs, which are naturally waterproof because they are designed as novel soft pneumatic actuators. Because a soft actuator has simple structural design and needs only one servomotor, the overall design of the prototype dog is very coMPact. This manuscript is not intended to demonstrate the dexterity of the robotic dog as no sensors and sophisticated control algorithms are designed and implemented into the prototype. A video showing the trotting and paddling of the prototype robotic dog is uploaded as a supplemental file (stacks.iop.org/BB/14/066008/mmedia).

There is still considerable improvement needed to the current prototype robotic dog design. The torso of the robotic dog is wide and square with a large drag coefficient, resulting in a large drag force when paddling. A streamline torso design can greatly reduce the drag coefficient, therefore reducing the drag force and increase the speed of the robot. Compared to the large trotting speed on land, the paddling speed of the robotic dog in water is relatively slow. This has been caused by the simple PCP soft actuator design and control. The soft actuator has only bending and extension deformation, making the power phase and recovery phase have the same limb path. As the paddling is a drag-based gait, the only parameter that can be controlled to reduce the drag force in recovery phase is the recovery speed. A small speed in recovery phase will extend the paddling cycle time. What's more, the bending of a limb will also induce varying lift forces (upward and downward). This force will induce pitching to the robotic dog. These drawbacks reduce the paddling efficiency for the robotic dog. For a real dog, the limb extend fully in power phase to maximize the thrust force, while in recovery phase, the limb are retracted close to the torso and greatly reduce the counter-productive drag force. For better paddling efficiency, more complex limb motion will be designed in the future.

Acknowledgments

Funding

This work was supported in part by the National Natural Science Foundation of China (NSFC) under Project 51805443.

ORCID iDs

Yunquan Li https://orcid.org/0000-0001-8425-2982

References

[1] Machado J T and Silva M F 2006 An overview of legged robots *Proc. of the 2006 Int. Symp. on Mathematical Methods in Engineering (Turkey)* pp 1–39

[2] Spröwitz A, Tuleu A, Vespignani M, Ajallooeian M, Badri E and Ijspeert A J 2013 Towards dynamic trot gait locomotion: design, control, and experiments with Cheetah-cub, a compliant quadruped robot *Int. J. Robot. Res.* **32** 932–50

[3] Raibert M, Blankespoor K, Nelson G and Playter R 2008 Bigdog, the rough-terrain quadruped robot *Proc. of the 17th Int. Federation of Automation Control (Korea)* pp 10822–5

[4] Ackerman E 2016 Boston Dynamics SpotMini Is All Electric, Agile, and Has a Capable Face-Arm *IEEE SPECTRUM* (https://spectrum.ieee.org/automaton/robotics/home-robots/boston-dynamics-spotmini)

[5] Seok S, Wang A, Chuah M Y, Otten D, Lang J and Kim S 2013 Design principles for highly efficient quadrupeds and implementation on the MIT Cheetah robot *IEEE Int. Conf. on Robotics and Automation (Germany)* pp 3307–12

[6] Hutter M 2013 StarlETH & Co.: design and control of legged robots with compliant actuation *PhD Thesis* ETH Zurich (https://doi.org/10.3929/ethz-a-009915229)

[7] Pongas D, Mistry M and Schaal S 2007 A robust quadruped walking gait for traversing rough terrain *IEEE Int. Conf. on Robotics and Automation (Italy)* pp 1474–9

[8] Zhang S, Liang X, Xu L and Xu M 2013 Initial development of a novel amphibious robot with transformable fin-leg composite propulsion mechanisms *J. Bionic Eng.* **10** 434–45

[9] Chen Y, Doshi N, Goldberg B, Wang H and Wood R J 2018 Controllable water surface to underwater transition through electrowetting in a hybrid terrestrial-aquatic microrobot *Nat. Commun.* **9** 2495

[10] Crespi A and Ijspeert A J 2009 Salamandra robotica: a biologically inspired amphibious robot that swims and walks *Artificial Life Models in Hardware* (London: Springer) pp 35–64

[11] Jun J Y and Clark J E 2015 Characterization of running with compliant curved legs *Bioinspir. Biomim.* **10** 46008

[12] Iida F, Rummel J and Seyfarth A 2008 Bipedal walking and running with spring-like biarticular muscles *J. Biomech.* **21** 656–67

[13] Galloway K C, Clark J E and Koditschek D E 2009 Design of a tunable stiffness composite leg for dynamic locomotion *ASME 2009 Int. Design Engineering Technical Conf. & Computers and Information in Engineering Conf. (USA)* pp 215–22

[14] Yu J, Ding R, Yang Q, Tan M, Wang W and Zhang J 2012 On a bio-inspired amphibious robot capable of multimodal motion *IEEE/ASME Trans. Mechatronics* **17** 847–56

[15] Prahacs C, Saudners A, Smith M K, McMordie D and Buehler M 2004 Towards legged amphibious mobile robotics *Proc. of the Canadian Design Engineering Network Conference (Canada)* pp 1–12

[16] Sun Y and Ma S E 2011 ePaddle mechanism: towards the development of a versatile amphibious locomotion mechanism *Proc. of the IEEE Int. Conf. on Intelligent Robots and Systems* pp 5035–40

[17] Harkins R, Ward J, Vaidyanathan R, Boxerbaum A X and Quinn R D 2005 Design of an autonomous amphibious robot for surf zone operations: part II-hardware, control implementation and simulation *IEEE/ASME Int. Conf. on Advanced Intelligent Mechatronics* pp 1465–70

[18] Hobson B W, Kemp M, Moody R, Pell C A and Vosburgh F 2005 Amphibious robot devices and related methods *US Patent No.* 6974356 (https://patents.google.com/patent/US6974356B2/en)

[19] Barrett D S, Triantafyllou M S, Yue D K P, Grosenbaugh M A and Wolfgang M J 1999 Drag reduction in fish-like locomotion *J. Fluid Mech.* **392** 183–212

[20] Zhang S, Zhou Y, Xu M, Liang X, Liu J and Yang J 2015 AmphiHex-I: locomotory performance in amphibious environments with specially designed transformable flipper legs *IEEE/ASME Trans. Mechatronics* **21** 1720–31

[21] Hirose S and Yamada H 2009 Snake-Like robots machine design of biologically inspired robots *IEEE Robot. Autom. Mag.* **16** 88–98

[22] Matsuo T, Yokoyama T, Ueno D and Ishii K 2008 Biomimetic motion control system based on a CPG for an amphibious multi-link mobile robot *J. Bionic Eng.* **5** 91–97

[23] Wright C, Buchan A, Brown B, Geist J, Schwerin M, Rollinson D, Tesch M and Choset H 2012 Design and architecture of the unified modular snake robot *Proc. of the IEEE Int. Conf. on Robotics and Automation* pp 4347–54

[24] Wang C, Xie G, Yin X, Li L and Wang L 2012 CPG-based locomotion control of a quadruped amphibious robot *Proc. of the IEEE Int. Conf. on Advanced Intelligent Mechatronics (Taiwan)* pp 1–6

[25] Dudek G *et al* 2007 Aqua: an amphibious autonomous robot *Computer* **40** 46–53

[26] Chin A 2010 AQUA2 underwater robot *Designboom* https://www.designboom.com/technology/aqua2-underwater-robot/

[27] Ijspeert A J, Crespi A, Ryczko D and Cabelguen J M 2007 From swimming to walking with a salamander robot driven by a spinal cord model *Science* **315** 1416–20

[28] Crespi A and Ijspeert A J 2008 Online optimization of swimming and crawling in an amphibious snake robot *IEEE Trans. Robot.* **24** 75–87

[29] Fish F E 1996 Measurement of swimming kinematics in small terrestrial mammals *Measuring Movement and Locomotion: From Invertebrates to Humans* ed K P Ossenkopp *et al* (London: Chapman & Hall) p 309

[30] Fish F E 1996 Transitions from drag-based to lift-based propulsion in mammalian swimming *Am. Zoologist* **36** 628–41

[31] Fish F E 1994 Influence of hydrodynamic-design and propulsive mode on mammalian swimming energetics *Aust. J. Zool.* **42** 79–101

[32] Li Y Q, Chen Y, Ren T, Li Y T and Choi S H 2018 Precharged pneumatic soft actuators and their applications to untethered soft robots *Soft Robot.* **5** 567–75

[33] Li Y Q, Chen Y H and Li Y T 2019 Pre-charged pneumatic soft gripper with closed-loop control *IEEE Robot. Autom. Lett.* **4** 1402–8

[34] Fish F E 1984 Mechanics, power output and efficiency of the swimming muskrat (*Ondatra zibethicus*) *J. Exp. Biol.* **110** 183–201

[35] Williams T M 1983 Locomotion in the North American mink, a semi-aquatic mammal. I. Swimming energetics and body drag *J. Exp. Biol.* **103** 155–68

[36] Dagg A I and Windsor D E 1972 Swimming in northern terrestrial mammals *Can. J. Zool.* **50** 117–30

[37] Davis W B 1942 Swimming ability of two small mammals *J. Mammal.* **23** 99

[38] Fish F E 2001 Mechanism for evolutionary transition in swimming mode by mammals *Secondary Adaptation of Tetrapods to Life in Water : Proc. of the Int. Meeting(Potiers, 1996)* ed J-M Mazin *et al* (Munchen: Verlag Dr. Friedrich Pfeil) pp 261–87

[39] Catavitello G, Ivanenko Y P and Lacquaniti F 2015 Planar covariation of hindlimb and forelimb elevation angles during terrestrial and aquatic locomotion of dogs *PLos One* **10** e0133936

[40] Milius S 2014 Life & evolution: Dog-paddle science debunks notion of underwater trot: From Newfoundlands to Yorkshire terriers, canines swim with similar, distinctive gait *Science News* **183** 10

[41] Lautrup B 2011 Buoyancy and Stability *Physics of continuous matter : exotic and everyday phenomena in the macroscopic world* (2nd edition) ed Lautrup B (Boca Raton: CRC press) pp 41–56

[42] Fish F E 2015 Dog paddle footfall data (https://digitalcommons.wcupa.edu/bio_data/1)

[43] Batchelor G K 2000 *An Introduction to Fluid Dynamics* (Cambridge, MA: Cambridge University Press) (https://doi.org/10.1017/CBO9780511800955)

[44] Huntley H E 1967 *Dimensional Analysis* (New York: Dover)

[45] Lee D V, Bertram J E and Todhunter R J 1999 Acceleration and balance in trotting dogs *J. Exp. Biol.* **202** 3565–73

[46] Carr B J and Dycus D L 2016 Canine gait analysis *Today's Veterinary Practice* **6** 93–100

[47] Hildebrand M 1985 Walking and running *Functional Vertebrate Morphology* ed M Hildebrand *et al* (Cambridge, MA: Belknap Harvard) pp 38–57